Cell Biochem Biophys (2010) 57:87–100
DOI 10.1007/s12013-010-9087-y

ORIGINAL PAPER

On the Structure-Bounded Growth Processes in Plant Populations

H. G. Kilian · M. Kazda · F. Király · D. Kaufmann · R. Kemkemer · D. Bartkowiak

Published online: 24 June 2010

Abstract If growing cells in plants are considered to be composed of increments (ICs) an extended version of the law of mass action can be formulated. It evidences that growth of plants runs optimal if the reaction–entropy term (entropy times the absolute temperature) matches the contact energy of ICs. Since these energies are small, thermal molecular movements facilitate via relaxation the removal of structure disturbances. Stem diameter distributions exhibit extra fluctuations likely to be caused by permanent constraints. Since the signal–response system enables in principle perfect optimization only within finite-sized cell ensembles, plants comprising relatively large cell numbers form a network of size-limited subsystems. The maximal number of these constituents depends both on genetic and environmental factors. Accounting for logistical structure–dynamics interrelations, equations can be formulated to describe the bimodal growth curves of very different plants. The reproduction of the S-bended growth curves verifies that the relaxation modes with a broad structure-controlled distribution freeze successively until finally growth is fully blocked thus bringing about "continuous solidification".

Keywords Plants · Population · Increment model · Optimized ensemble structure · Growth process · Relaxation-frequency dispersion · Growth logistics · Communities

H. G. Kilian (✉)
Abteilung Experimentelle Physik, Universität Ulm,
Albert-Einstein Allee 11, 89069 Ulm, Germany
e-mail: hanns-georg.kilian@uni-ulm.de

M. Kazda
Institut für Systematische Botanik und Ökologie,
Universität Ulm, Albert-Einstein Allee 11, 89069 Ulm, Germany
e-mail: marian.kazda@uni-ulm.de

F. Király
Institut für Reine Mathematik, Universität Ulm,
Helmholtzstraße 18, 89081 Ulm, Germany
e-mail: franz.kiraly@uni-ulm.de

D. Kaufmann
Institut für Humangenetik, Universitätsklinik,
Albert-Einstein Allee 11, 89081 Ulm, Germany
e-mail: dieter.h.kaufmann@uni-ulm.de

R. Kemkemer
Max-Planck-Institut für Metallforschung,
Heisenbergstr. 3, 70569 Stuttgart, Germany
e-mail: ralf.kemkemer@mf.mpg.de

D. Bartkowiak
Klinik für Strahlentherapie und Radioonkologie,
Universitätsklinikum, Albert-Einstein-Allee 23,
89081 Ulm, Germany
e-mail: detlef.bartkowiak@uniklinik-ulm.de

Introduction

The growth process of plants and plant populations has been studied intensively [1–12]. In any case, stands of plants show sigmoidal growth curves [4]. A key point of a description is to relate this behaviour to the properties of the individuals [13]. Many growth models have been developed [14] some of them typified by the two factors proportional to (1) increasing tree size and (2) the decline of trees resulting from competition, diseases, or other disturbances. Growth-related molecular details have been investigated such as the process of irreversible cell wall extension [15]; however, despite these achievements description of the growth process remains incomplete. The observation that growth curves of plants fit to several

general equations [14] is symptomatic of the difficulty to come to an unambiguous characterization [8].

This situation motivated us to apply a previously described increment model [16–18]. Increments (ICs) are equivalent molecule clusters cells are composed of. A major advantage is that the actual molecular processes of forming an IC need not be discussed since ICs are assumed to be preformed in the environment or in a reservoir. Cell growth via IC absorption can thus be treated like a chemical reaction. Linked in a cell the ICs hold together via isoenergetic contacts. These are so weak that the configuration of the IC piles fluctuates by thermal activation. Growth processes are enabled to adjust optimal conditions. Putting this in concrete terms the fundamental law results that under stationary conditions the reaction–entropy term (entropy times the absolute temperature) of the increments has to match the contact energy. Yet, this balance is realizable only when a cell-size distribution is formed. The configuration of these patterns fluctuates caused by cell growth and division. Cells of different size are thus stirred all the time providing mixing entropy [16–18]. Hence, the laws of the thermodynamically founded reaction kinetics determine essential properties of the superstructure. Moreover, fitting experimental data with the equations it can be deduced that [16–18] different cell types exhibit altogether analogous size distributions.

Of course, when an IC is integrated in a cell, the steady-state conditions are disturbed. Optimal growth conditions must be readjusted via broad-band molecular relaxation. Each growing cell within an ensemble emits signals, e.g. by membrane oscillations [16, 19] thus indicating its presence and condition. The superposition of all signals within a population leads to a modulated field typified by a frequency that increases with the cell number. On the other hand, the distribution of relaxation times that determine molecular rearrangements remains constant. When due to rising cell numbers the interval between signals grows shorter than the relaxation time of a given mode, this mode becomes blocked. Starting with the slowest highly cooperative mode, all subsequent growth-relevant rearrangements are frozen. This phenomenon of relaxation-frequency dispersion leads to S-shaped growth curves, irrespective of the underlying genetic background or individual factors. The phenomenon explains that optimal conditions can be achieved only in ensembles below a maximum cell number. This limit depends to a certain extent on the genetically encoded molecular composition and on environmental conditions [16–18].

The aim of this study is to use the IC model to describe the growth processes and the superstructure development in plants and plant populations. Here, we pay attention to the existence of a network of finite-sized subsystems. The growth of all these subsystems is expected to be controlled by the same logistics because the model should apply to the level of cellular, organismic and population growth. Consistent applications throughout numerous plant species and even in naturally growing multi-species populations underline the usefulness of this characterization.

Environmental or genetic alteration should enforce a readjustment of optimized distributions. Experimental manipulations of these conditions in individuals are predicted to be integrated in the ensemble structure and consequently influence the ensemble's growth. According to the underlying principles, even the species composition of plant societies for example studied in various tropical rain forests [20] should be optimized patterns. This may help to explain how the superstructure of abundant species is developed.

The Cell-Size Distribution

The deduction of the basic relations has previously been shown in detail [16–18]. The cell-size distribution as function of the number n_y of IC-to-IC contacts is given by Eq. 1:

$$n_y = \xi(y - y_{\min})^p \exp\{-\beta(y - y_{\min})\Delta u_0\}$$
$$y_{\min} \le y \le y_{\max};\ \xi = \sum_{y_{\min}}^{y_{\max}} n_y;\ \beta = (k_B T)^{-1} \quad (1)$$

Equation 1 is the analytical formulation of the mass-action law extended to a very large number of reactions. The distributions are optimized patterns. $y_{\min}$ and $y_{\max}$ represent the observed size extremes, Δu_0 is the contact energy per increment linked in a cell. k_B is Boltzmann's constant, T is the absolute temperature. The parameter ξ is the total number of the constituents. The value of $y_{\min}$ determines the position but not the shape of the distribution which is thus determined by p and $\beta\Delta u_0$ exclusively.

Depending on intracellular structure fluctuations p seems to adopt values of $0 \le p \le 3$. At $p = 3$ the intracellular entropy should be maximal. Extremely small values ($p \le 1$) are expected in self-assembled highly anisotropic protein complexes [21].

As function of the dimensionless variable $\eta = (y - y_{\min})\Delta u_0/k_B T = (y - y_{\min})\beta\Delta u_0$ these master curves come about [16–18]

$$\Phi(\eta, p) = x_y/C_A = \eta^p \exp\{-\eta\}$$
$$C_A = \xi/[\beta\Delta u_0]^p \quad (2)$$

$\Phi(\eta, p)$ depends exclusively on the value of p.

A Significant Test

The frequency distributions of cells n_y within tubuli of two meristems shown in Figs. 1 and 2 can be described with Eq. 1. The solid lines are calculated with parameters determined by a nonlinear fitting program (Appendix).

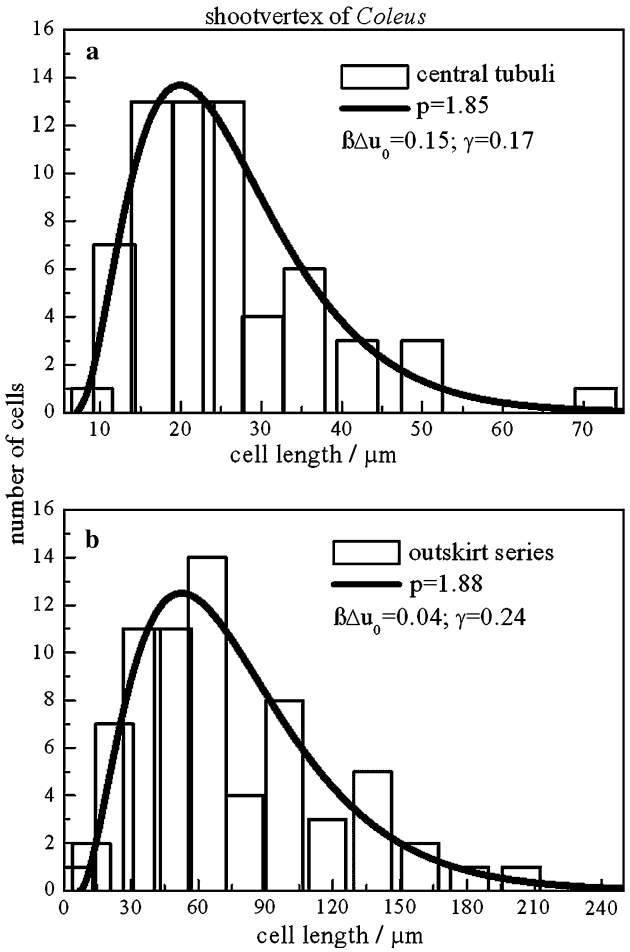

Fig. 1 **a** Cell length (µm) in central tubuli; **b** cell length (µm) outskirt tubuli. The *bold lines* are calculated with Eq. 1

Cell-length distributions in the shoot vertex of *Coleus* [22] (Fig. 1) and in the root meristem of *Medicago truncatula* [23] (Fig. 2) are typified by $\langle p \rangle = 1.86$. Since both meristems show anisotropic cell configurations this value is plausible. $\langle \gamma \rangle = 0.27$ characterizes extra fluctuations caused by aberrant data points.

Definitions and Relations

The Relaxation Time

Intracellular processes run rapidly and are strictly coordinated. The relaxation of a cell is thus described by an exponential function with a single relaxation time [24]. In an unorthodox manner the relaxation time τ_y of cells with y IC-to-IC contacts is defined as product of the "relaxation-mode factor" τ_{0y} times the "kinetic factor" τ_{kin} [25].

$$\tau_y = \tau_{0y}\tau_{\mathrm{kin}} \tag{3}$$

τ_{0y} counts the number of relaxation modes in cells with y IC-to-IC-contacts that increases with the cell size due to the growing number of micro-states [16–18]. The relaxation-mode distribution formulates strict interrelations between structure and dynamics. On the other hand, τ_{kin} refers to the structure-independent local dynamics.

The Interrelation Between ω_c and t

If in a growing subsystem each cell emits signals with the frequency ω_0, the frequency ω_c within an ensemble composed of $n_c'(t)$ cells is then equal to [16–18]

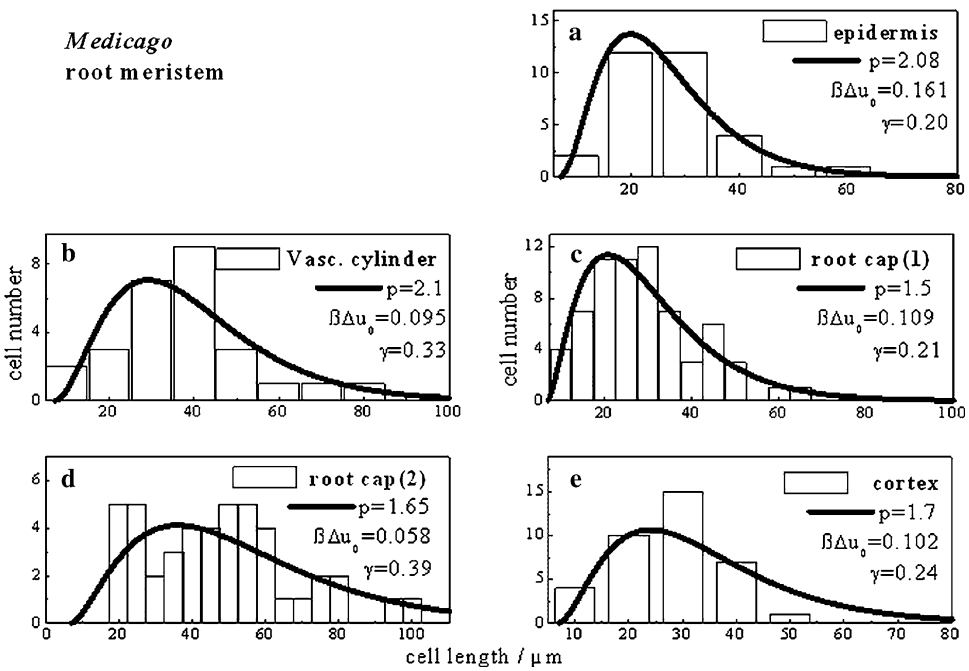

Fig. 2 Cell-length distributions deduced from measurements of Holmes et al. [23]. **a** epidermis, **b** vascular cylinder, **c** root cap (1), **d** root cap (2), (**e**) cortex. The *solid lines* are computed with the use of Eq. 1

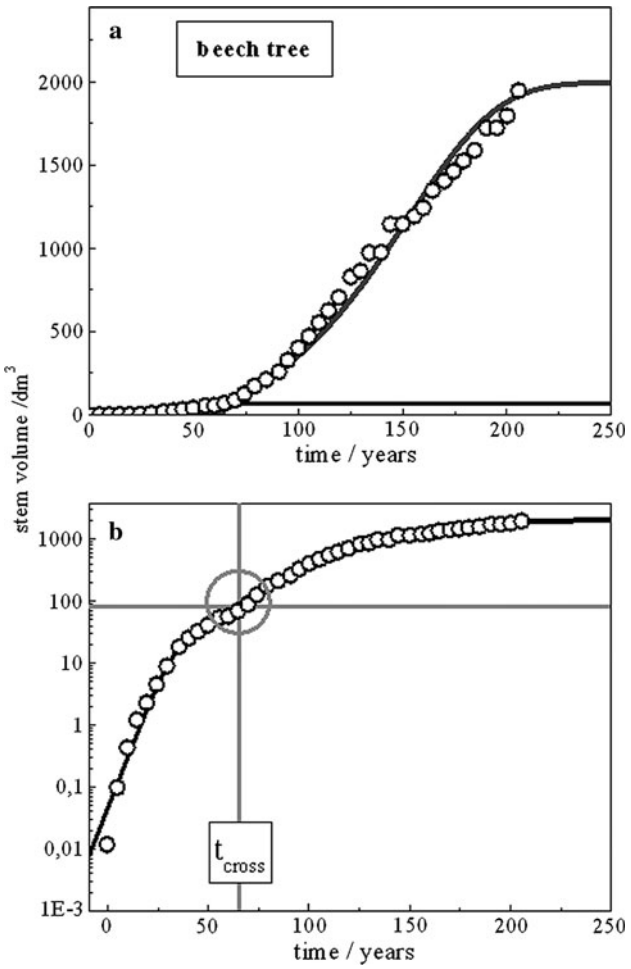

Fig. 3 The stem volume without bark measured by Hozumi [34] in beech trees as function of the age (given in years). The *bold line* is calculated with Eq. 10 and the parameters in Table 1. t_{cross} indicates the transition from vegetative to generative growth: **a** linear plot, **b** logarithmic plot

$$\omega_c(t) = \omega_0 n'_c(t) = \omega_0 2^{t/t_{c0}} = \omega_0 \exp\{\ln(2)(t/t_{c0})\}$$

t_{c0} is the time required to double the number of cells $n'_c(t)$. Yet, the interrelation between the time t and the signal frequency ω_c is given by [17, 18]

$$t = t_c \ln\left(\frac{\omega_c}{\omega_0}\right). \tag{4}$$

Hence, the "real" doubling time t_c should be equal to $t_c = t_{c0}/\ln(2) = 1.44\, t_{c0}$. Communication among all cells within a cell ensemble thus needs a signal frequency $\omega_c/\omega_0 = \exp\{t/t_c\}$ that grows exponentially in the course of time.

Symmetries

Since cell ensembles show cell-size distribution, relaxation-mode distribution arises (Eq. 3). These symmetries can be formulated [16–18]

Table 1 Growth-invariant parameters of the bimodal growth curve of stem volume of a beech tree according to Hozumi [34]

Vegetative		Generative	
Doubling time (Eq. 3)			
t_{c1}	10.5 years	t_{c2}	22 years
Maximum value of the stem volume (dm^3)			
$\Delta n'_{c1}$	70	$\Delta n'_{c2}$	2.000
Kinetic factor of the relaxation time (years)			
τ_{kin1}	0.0011	τ_{kin2}	0.00055
Upper limit of the relaxation-mode spectrum			
$\ln(\tau_{0\text{ymax1}})$	4	$\ln(\tau_{0\text{ymax2}})$	8

$p = 3$; $t_{\text{cross}} = 65$ years; $t_{c2}/t_{c1} = 2.1$

$$\Phi(\eta, p) = \Phi\big(\Delta s_y/k_B, p\big) = \Phi\big(\ln(\tau_{0y}), p\big); \quad p = \text{const} \tag{5}$$

with

$$\Phi(\eta, p) = \eta^p \exp\{-\eta\}$$
$$\Phi\big(\Delta s_y/k_B, p\big) = \big(\Delta s_y/k_B\big)^p \exp\big\{-\Delta s_y/k_B\big\}$$
$$\Phi(\ln(\tau_{0y}, p)) = \ln^p\big(\tau_{0y}\big)/\tau_{0y}.$$

The identity $\Phi(\eta, p) = \Phi(\Delta s_y/k_B, p)$ demands that contact energy and entropy are strictly interrelated. The relation $\Phi(\ln(\tau_{oy}), p) = \Phi(\eta, p)$ formulates the model's typical unambiguous structure–dynamics interrelation. Of course, cell ensembles in plants should exhibit these symmetries, too.

The Relaxation-Frequency Dispersion

The signal system in a growing plant population embraces numerous contributions [26–29] including transmembrane receptors, G-protein-coupled signals, communication during cell division, interaction among leaves, pressure variation in liquid cords, stress impulses, interaction of penetrating roots, etc. Until now, descriptions of growth do not directly account for all these phenomena.

Referring to Pelling et al. [19], we use a mean-field approximation by assuming that signals are transported via a stress field. During growth, deformations come about; relaxation has to reinstall optimal process conditions. During these processes, energy is stored but also dissipated. The frequency dependence is described by the complex shear modulus $G^*_y(\omega_c)$, at a signal-field frequency ω_c defined as the sum of the real part $G'_y(\omega_c)$ and the imaginary component $G''_y(\omega_c)$ [30]. We use then the normalized complex function $X^*_y(\omega_c, \tau_y)$ [17]

$$X^*_y\big(\omega_c\tau_y\big) = X'_y\big(\omega_c\tau_y\big) + iX''_y\big(\omega_c\tau_y\big)$$
$$X'_y\big(\omega_c\tau_y\big) = \frac{G'_y}{\Delta G'} = \frac{\omega_c^2\tau_y^2}{1+\omega_c^2\tau_y^2} \tag{6}$$
$$X''_y(\omega_c\tau) = \frac{G''_y}{\Delta G'} = \frac{\omega_c\tau_y}{1+\omega_c^2\tau_y^2}$$

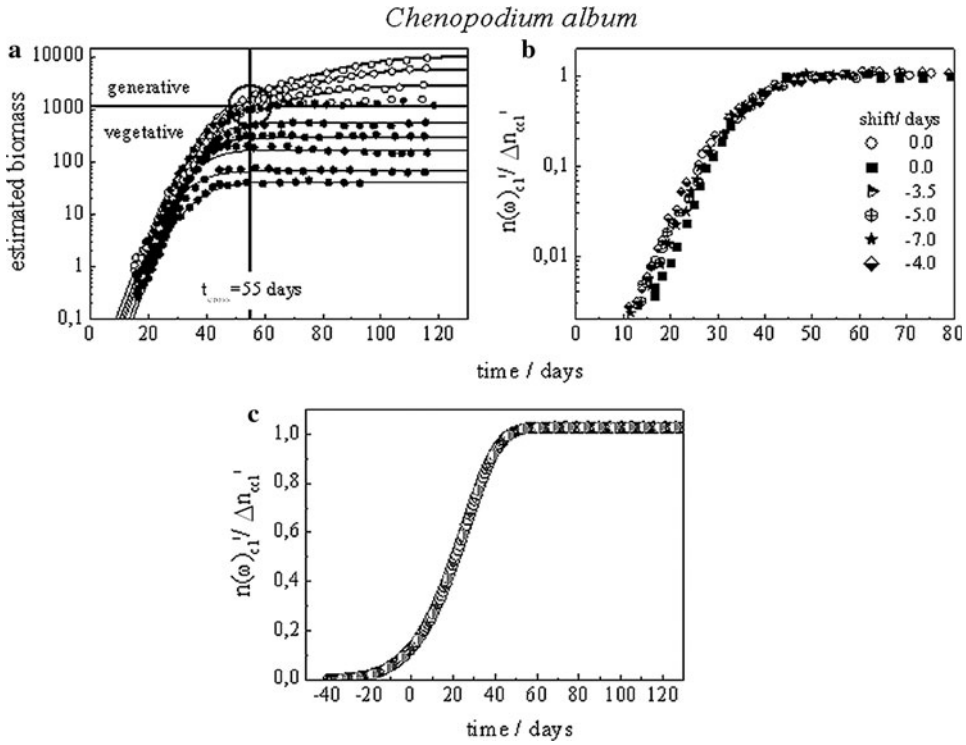

Fig. 4 **a** Biomass of *Chenopodium album* (height × diameter^2) in arbitrary units for individual plants growing at 400 plants/m^2 according to Damgaard et al. [7]. The *bold lines* are calculated with Eq. 10 using the parameters in Table 2. t_{cross} indicates the transition from vegetative to generative growth. **b** Normalized biomass (n_{cc1}'/ $\Delta n_{cc1}'$) from the vegetative phase as function of time (days). To allow optimal comparison of their shape, the curves are slightly shifted along the *x*-axis. **c** Overlay of calculated normalized biomass (Eq. 10)

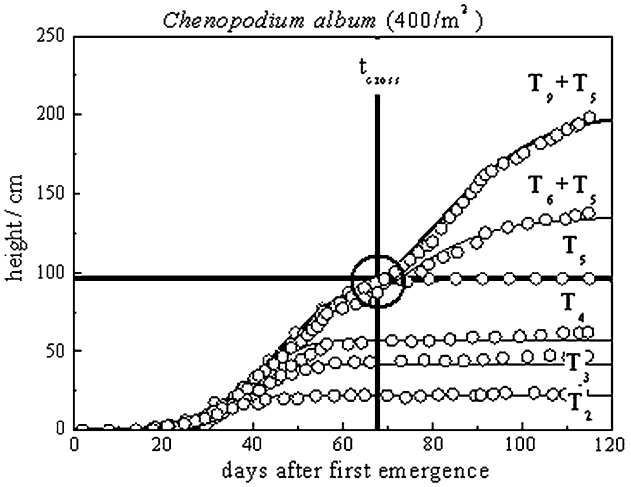

Fig. 5 Selected data from height measurements of *Chenopodium album* individuals in a stand of 400 plants/m^2 according to Nagashima et al. [36]. The *bold lines* are computed with Eq. 10 and the parameters in Table 3. t_{cross} indicates the transition from vegetative to generative growth. The maximum height in the vegetative regime amounts to about 100 cm. Note the bimodal curves $T_6 + T_5$ and $T_9 + T_5$

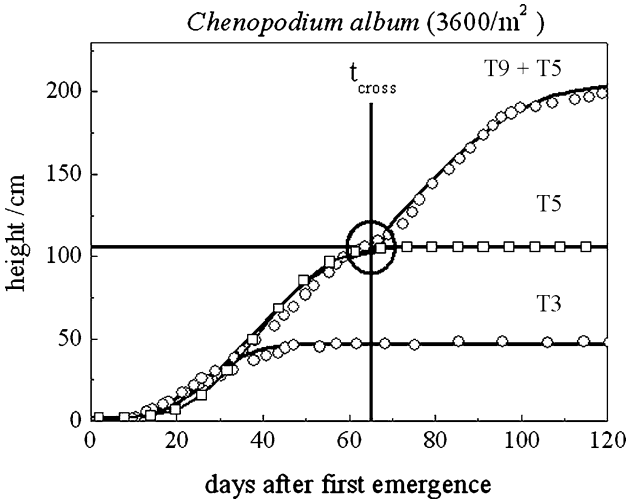

Fig. 6 Selected data from height measurements of *Chenopodium album* individuals in stands of 3,600 plants/m^2 according to Nagashima et al. [36]. The *bold lines* are computed with Eq. 10 and the parameters from Table 4. Irrespective of the increased population density, the individual transition from vegetative to generative growth occurs around 65 days of age and 100 cm of height

$\Delta G' = G'_{max} - G'_{min}$ defines the "relaxation strength" as difference between the maximum modulus G'_{max} at very high frequencies and G'_{min} as the static minimum. These functions are appropriate for characterizing sigmoidal growth curves. Due to the relaxation-frequency dispersion all-embracing communication in cell ensembles is only possible if the number of constituents is smaller than a specific maximum [16–18]. The cell number in plants exceeds by far this limit. The whole plant shows thus a superstructure, constituted by finite-sized subsystems as widely autonomous cell ensembles.

The Growth Process

The normalized relaxation-mode distribution $h_y(\ln(\tau_{0y}), p)$ is introduced:

Table 2 Growth-invariant parameters of monomodal growth curves in the vegetative regime and bimodal patterns at times beyond the transition around $t_{cross} = 55$ days found by estimating the biomass of single *Chenopodium* plants in a population with the density of 400/m^2 according to Damgaard et al. [7]. Apart from $\Delta n'_{cc1}$ and $\Delta n'_{cc2}$ the values of the parameter sets of the individual plants in the vegetative and the generative regime do not change much

No.	Max. biomass		Kinetic relaxation		Doubling time	
	$\Delta n_{cc1}{}'$	$\Delta n_{cc2}{}'$	τ_{kin1} (days)	τ_{kin2} (days)	t_{c1} (days)	t_{c2} (days)
9 + 6	1,100	11,580	3.4×10^{-5}	4.5×10^{-5}	6	12
8 + 6	1,100	5,877	10^{-4}	4.5×10^{-5}	6	12
7 + 6	1,100	2,800	2×10^{-5}	6×10^{-4}	6	12
6	1,100		2×10^{-5}		6	
5	562		7×10^{-5}		6	
4	228		9×10^{-5}		6	
3	166		9×10^{-5}		6	
2	66		9×10^{-5}		6	
1	41		9×10^{-5}		6	

$p = 3$; $t_{cross} = 55$ days; $\ln(\tau_{0ymax1}) = 4$; $\ln(\tau_{0ymax2}) = 12$; $t_{c2}/t_{c1} = 2$

Table 3 The growth-invariant parameters (400/m^2) of the growth curves (Fig. 5) of *Chenopodium album* plants

No.	t_{ck} (days)	τ_{kink} (days)	$\Delta n'_{cck}$	$\ln(\tau_{0ymaxk})$
T2	8.5	3.3×10^{-3}	22	4
T3	8.5	1.8×10^{-3}	45	4
T4	8.5	1.2×10^{-3}	60	4
T5	9.5	1.5×10^{-3}	92	4
T6 (+T5)	18	1.5×10^{-3}	135	12.5
T9 (+T5)	18	3.3×10^{-3}	200	12.5

$p = 1$; $t_{cross} = 65$ days; $\ln(\tau_{0ymax1}) = 4$; $\ln(\tau_{0ymax2}) = 12$; $t_{c2}/t_{c1} = 1.9$

$$h_y\left(\ln\left(\tau_{0y}\right),p\right) = \Phi\left(\ln\left(\tau_{0y}\right),p\right) \Big/ \sum_{\tau_{0y\,min}}^{\tau_{0y\,max}} \Phi\left(\ln\left(\tau_{0y}\right),p\right) \qquad (7)$$

$\tau_{0y\,min}$ and $\tau_{0y\,max}$ are the lower and upper limits of the mode spectrum, respectively. Considering the growth of a cell ensemble as a linear process, the total cell number $n'(\omega_c)$ or $n''_c(\omega_c)$ is obtained by adding all fractions $h_y(\ln(\tau_{0y}),p)$ of differently large cells multiplied by the conjugated functions $X'_y(\omega_c)$ and $X''_y(\omega_c)$ (Eq. 6). An ensemble of finite-sized widely autonomous subsystems is formed. The S-bended shape of $X'_y(\omega_c)$ is a consequence of the freezing of molecular motions during growth which leads to solidification of the superstructure. The dissipation function $X''_y(\omega_c)$ passes a maximum at $(\omega_c\tau_y) = 1$ where the growth rate is maximal. Calling the maximum number of cells in a grown-up subsystem $\Delta n'_c$, the cell number $n'_c(\omega_c)$ and the corresponding loss $n''_c(\omega_c)$ are equal to

$$\begin{aligned} n'_c(\omega_c) &= 1 + \sum_y n'_{cy}(\omega_c) = 1 + \Delta n'_c \sum_y h_y\left(\ln(\tau_{0y}),p\right) X'_y\left(\omega_c\tau_y\right) \\ n''_c(\omega_c) &= \sum_y n''_{cy}(\omega_c) = \Delta n'_c \sum_y h_y\left(\ln(\tau_{0y}),p\right) X''_y\left(\omega_c\tau_y\right) \end{aligned} \qquad (8)$$

Growth of Individual Plants in a Population

Irrespective of the cell type, all subsystems in a plant should show the same growth logistics [17]. As approximation, we assume synchronized growth of all these constituents. For n_0 subsystems growing altogether up to $\Delta n'_c$, $n'_c(\omega_c)$ and $n''_c(\omega_c)$ are equal to:

$$\begin{aligned} n'_c(\omega_c) &= \sum_{i=1}^{n_0} n'_{ci}(\omega_c) = n_0 \Bigg(1 + \Delta n'_c \sum_y h_y\left(\ln(\tau_{0y}),p\right) \\ &\quad \times X'_y\left(\omega_c\tau_y\right) \Bigg) \\ n''_c(\omega_c) &= \sum_{i=1}^{n_0} n''_{ci}(\omega_c) = n_0 \Delta n'_c \sum_y h_y\left(\ln(\tau_{0y}),p\right) X''_y\left(\omega_c\tau_y\right) \end{aligned} \qquad (9)$$

with

$$\Delta n'_c = \sum_{i=1}^{n_0} \frac{\Delta n'_{ci}}{n_0};\ n'_{c\,min} = n_0;\ n'_{c\,max} = n_0\left(1 + \Delta n'_c\right).$$

The absolute values of $\Delta n'_c$, n_0, t_c, τ_{kin}, p depend on individual genetic factors and on the environmental conditions.

Bimodal Growth

We consider here the growth of single plants which passes at a defined age from the vegetative into the generative phase. Of course, in both regimes the growth is amenable

Table 4 The growth-invariant parameters of the growth curves (Fig. 6) of individuals of *Chenopodium album* in a population at 3,600 plants/m^2

No	Doubling time, t_c (days)	Kinetic relaxation factor, τ_{kin} (days)	Max. height, $\Delta n_{cck}{}'$
T3	8.5	6×10^{-3}	47
T5	10.5	5×10^{-3}	100
T9 + T5	19	5×10^{-3}	205

$p = 1$; $t_{cross} = 65$ days; $\ln(\tau_{0ymax1}) = 4$; $\ln(\tau_{0ymax2}) = 12.5$; $t_{c2}/t_{c1} = 2.2$

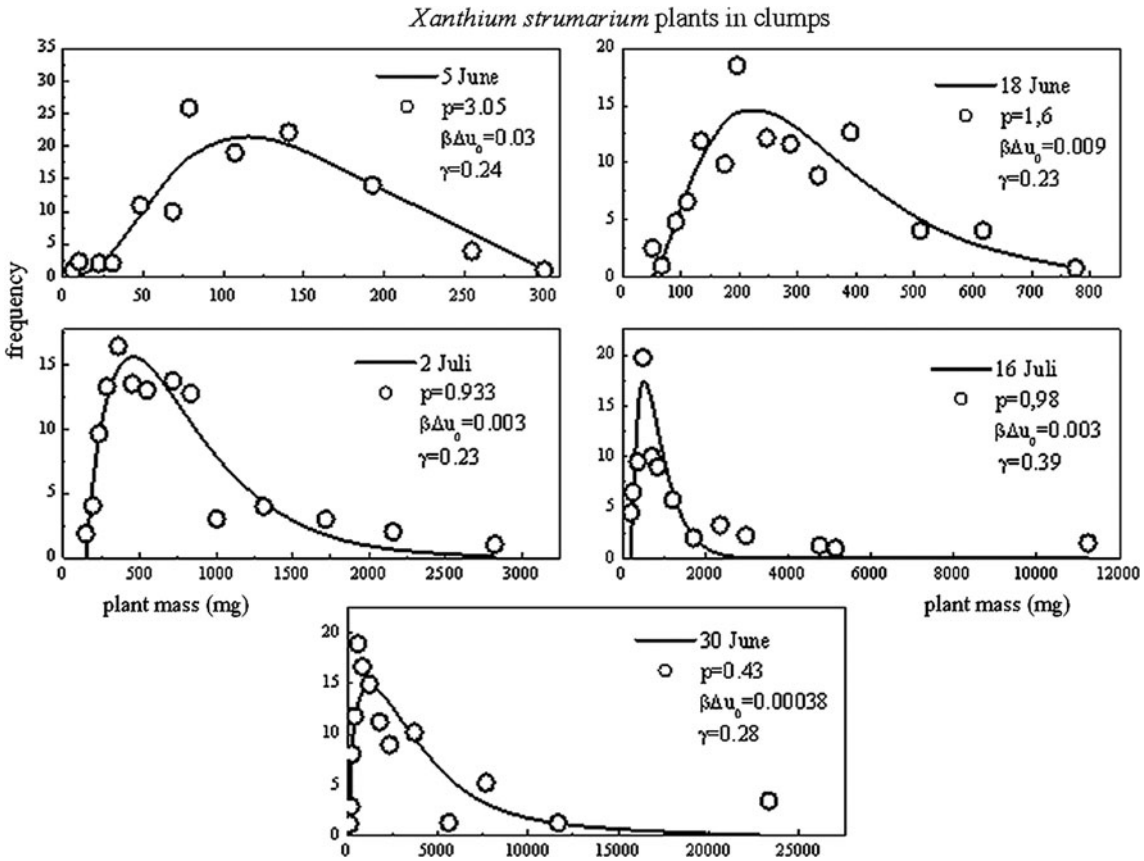

Fig. 7 **a–c** Frequency distributions of estimated biomass of *Xanthium strumarium* plants growing in clumps as measured at different ages by Weiner et al. [4]. The plots are based on 15 intervals. The *solid lines* are obtained with Eq. 1

to the same logistics. According to the relaxation-frequency dispersion, vegetative growth ends at a maximum number of cells. By switching to the generative growth mode, further gain of biomass follows a differently parameterized process as a consequence of shifted allocation of nutrients towards reproductive structures. This transition is known to depend on the action of flowering-period genes [31, 32]. Being aware of the complexity of growth and allocation modeling [33], we treat the transition as occurring around t_{cross}. During the transition, parameters adopt new values that afterwards remain constant, i.e. within the whole generative growth regime the topological characteristic of the superstructure is growth invariant. Bimodal growth patterns can be described with these relations:

$$n'(\omega_c) = \left[n'_{c1}\right]_{t=0}^{t_{\mathrm{cross}}} + \left[n'_{c2}\right]_{t_{\mathrm{cross}}}^{t_{\max}}$$

$$n'_{ck}(\omega_c) = \sum_{i=1}^{n_{0k}} n'_{cik}(\omega_c) = n_{0k} \times \left(1 + \Delta n'_{ck} \sum_y h_{yk}\left(\ln\left(\tau_{0yk}\right), p\right) X'_{yk}\left(\omega_c \tau_{yk}\right)\right)$$

$$n'_{ck}(\omega_c) = n_{0k} + \Delta n'_{cck} \sum_y h_{yk}\left(\ln\left(\tau_{0yk}\right), p\right) X'_{yk}\left(\omega_c \tau_{yk}\right) \quad (10)$$

with

$$\Delta n'_{cck} = n_{ok}\Delta n'_{ck};\ \Delta n'_{ck} = \sum_{i=1}^{n_{0k}} \frac{\Delta n'_{cki}}{n_{0k}};\ k = 1, 2$$

$\Delta n'_{cik}$ gives the maximal cell number in the ith subsystem in the kth growth regime ($k = 1$, vegetative mode; $k = 2$, generative mode). Since $\Delta n'_{ck}$ is relatively large ($\Delta n'_{ck} \gg 1$, $k = 1,\ 2$), the maximum cell number is $n'_{cck} = n_{ok}(1 + \Delta n'_{ck}) \approx n_{0k}\Delta n'_{ck}$. All combinations n_{0k} and $\Delta n'_{ck}$ with the same value $n_{0k}\Delta n'_{ck}$ are equivalent, i.e. absolute values of both parameters cannot be deduced from the growth curve.

Extensive quantities like the volume or the biomass should increase proportional to the cell number. Hence, defining adequate scaling factors, the growth of biomass or volume of a plant can be described with Eq. 10. The number $n'(t)$ is obtained by plotting $n'(\omega_c)$ against t defined in Eq. 4.

Experimental Results and Discussion

The Growth of a Beech Tree

The growth of the stem volume of a beech tree published by Hozumi [34] is depicted in Fig. 3a, b. The solid lines are

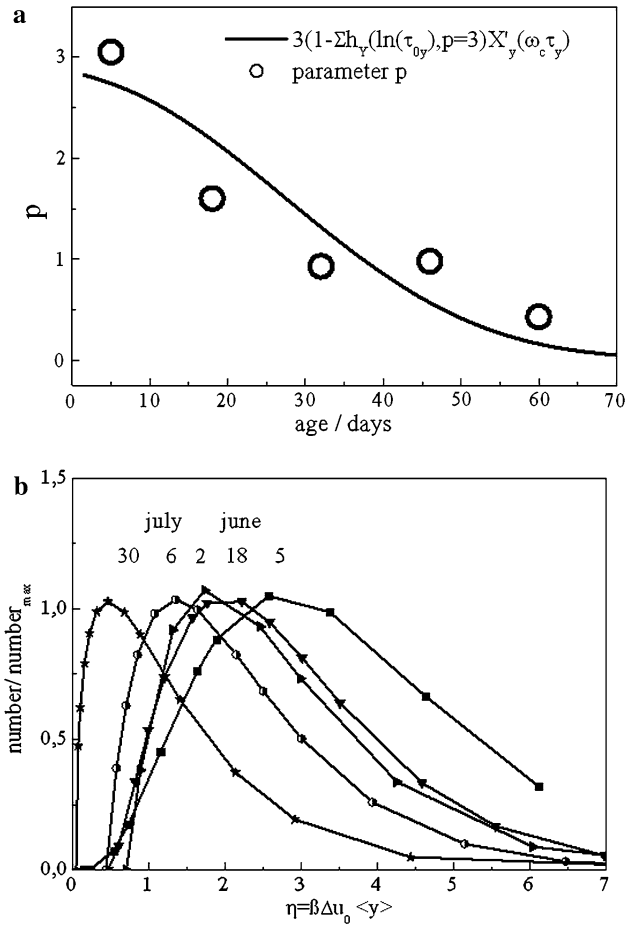

Fig. 8 **a** The parameter p during growth. The curve is computed with the indicated relation. **b** Normalized-size distributions of *Xanthium strumarium* at different ages. Error values γ are indicated

calculated with Eq. 10 and the parameters in Table 1. Referring to previous findings [16–18], the parameter p is assigned the value of three. Equation 10 implicates the growth-induced freezing of the intracellular dynamics. It describes the growth as an irreversible process nearest to the optimal state of reference. Linear reaction kinetics can therefore be applied in these multi-component multi-reaction systems. When vegetative growth starts, the parameters quickly adopt values that stay constant until the system switches to the generative growth regime. Readjusted during the transition, these values do not change any more. It is not clear how and why the optimal number of subsystems is "nucleated" at the start of each growth mode.

Vegetative growth ($k = 1$) shows a small mode-spectrum with an upper limit of $\ln(\tau_{y0\,\max 1}) = 4$ while in the generative regime it is equal to $\ln(\tau_{y0\,\max 2}) = 8$. According to Eq. 4 the ratio of $\ln(\tau_{y0\,\max 2})/\ln(\tau_{y0\,\max 1}) = 2$ means that the width of the cell-size distribution in the generative phase should be twice that of the vegetative regime. This is in line with the finding that the ratio of the doubling times is also equal to $t_{c2}/t_{c1} = 2.1$ (Table 1).

Let us use the relation $(\omega_{ck}/\omega_0) = \exp\{t_{\text{cross}}/t_{ck}\}$ (see Eq. 4) to calculate the growth-invariant signal frequencies at $t_{\text{cross}} = 65$ years. In the vegetative regime the value of $(\omega_{c1}/\omega_0)_{\text{cross}/tc1} = 488$ again exceeds substantially the value in the generative phase $(\omega_{c2}/\omega_0)_{\text{cross}/tc2} = 19.5$. In the generative regime, optimization is thus achieved at relatively low signal frequencies. Extrapolating the calculation with Eq. 10, a beech tree is predicted to be grown-up at 200–250 years which is in good accord with 200–300 years that is found for *Fagus sylvatica* L. (http://de.wikipedia.org/wiki/Rotbuche).

Hence, structure development and growth dynamics in a growing tree are strictly connected at any time.

Growth of *Chenopodium album* Plants

Here, we describe the growth of the biomass of individuals in a *Chenopodium album* population studied by Damgaard et al. [7] (Fig. 4) and their height distributions published by Nagashima et al. [35] (Figs. 5, 6). To fit the biomass growth curve we set $p = 3$ while the height growth curves are reproduced with $p = 1$. This is plausible since in bundles of irreversibly elongated cells, only small longitudinal fluctuations can be activated.

In the vegetative growth regime the relaxation-mode spectrum is narrow $(\ln(\tau_{y0\,\max 1}) = 4)$ while in the generative regime we found $\ln(\tau_{0y\,\max 2}) = 12$. This agrees with values as determined in cell cultures $(\ln(\tau_{y0\,\max}) = 12.7 : \tau_{y0\,\max} = 3.3 \times 10^5)$ [16–18].

Tables 2, 3, 4 evidence that even when $\Delta n'_{cc1}$ and $\Delta n'_{cc2}$ change substantially all the other parameters are hardly modified; specifically t_{ck} always shows the same order of magnitude. The ratio of the doubling times falls in the range of $t_{c2}/t_{c1} = 1.9$–2.2. At t_{cross} these signal frequencies are:

biomass: $(\omega_{c1}/\omega_0)_{t_{\text{cross}}/t_{c1}} = 9,572,\ (\omega_{c2}/\omega_0)_{t_{\text{cross}}/t_{c2}} = 97$

height: $(\omega_{c1}/\omega_0)_{t_{\text{cross}}/t_{c1}} = 2,097,\ (\omega_{c2}/\omega_0)_{t_{\text{cross}}/t_{c2}} = 37.$

Hence, the vegetative phase shows narrow relaxation-mode distributions while it is broad in the generative phase.

Finding the same growth logistics in the vegetative and in the generative regime does not explain the transition. Well-directed genetic factors seem to be necessary. Not before the vegetative growth is totally blocked $[(\Delta n'_{cc1})_{\max} = \text{const}]$ does the flowering-period genes [27] succeed in activating this transition. The intersecting lines in Figs. 3, 4, 5, 6 are inserted to highlight the similarity of the transition in vastly different plants like trees and herbs.

Symmetries

Figure 4b (Table 2) shows that in the vegetative regime all data fall in one master curve. Together with the pattern

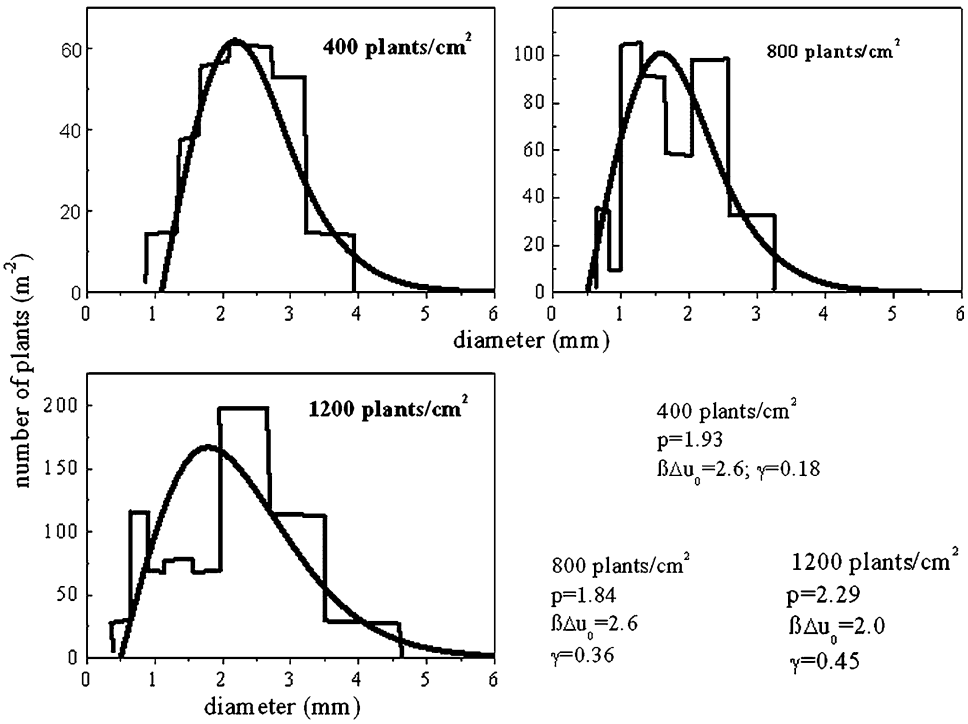

Fig. 9 Frequency distributions of the diameter of even-aged *Chenopodium album* plants in stands with different initial densities (Nagashima et al. [35]). The *bold lines* are calculated with the Eq. 1 and the parameters as indicated

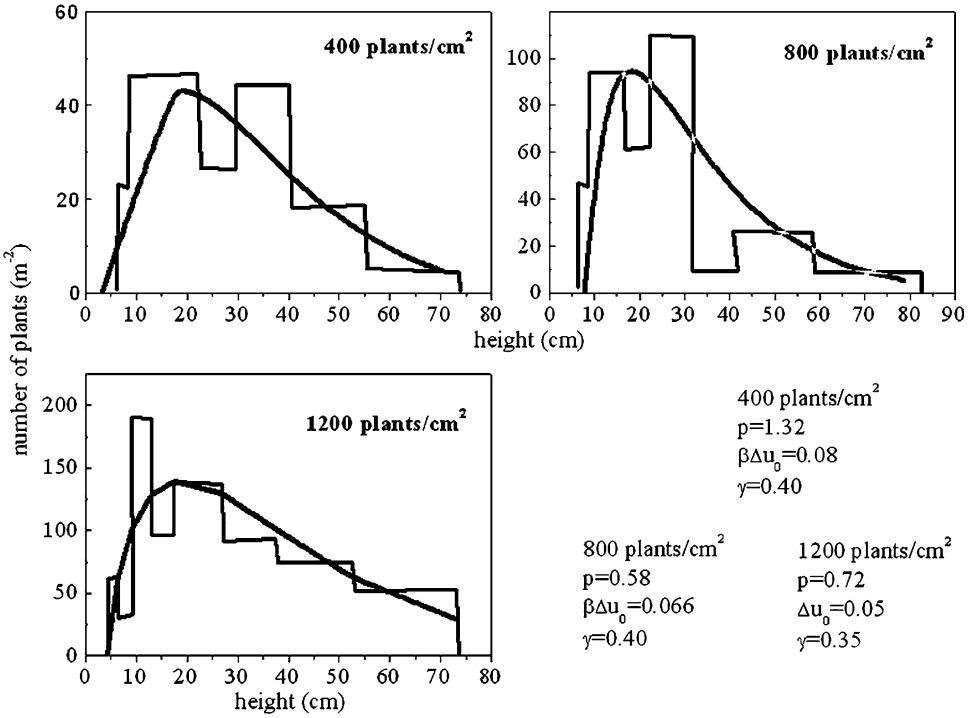

Fig. 10 Frequency distributions of *Chenopodium album* plant height from stands with different initial densities, according to Nagashima et al. [35]. The *bold lines* are calculated with Eq. 1 and the parameters as indicated

derived in Fig. 4c striking similarities are evident: since the doubling times are the same, the signal frequencies ω_{c1} (Eq. 4) are also identical. Despite different numbers of subsystems [13] all these plants accomplish vegetative growth at $t_{\text{cross}} \cong 55$ days. The relatively sharp bending at the end results from the narrow relaxation-mode distribution $(\ln(\tau_{0y\max 1} = 4)$. Hence, all growth curves can be fitted de facto by exclusively adjusting $\Delta n'_{cc1}$ (Table 2).

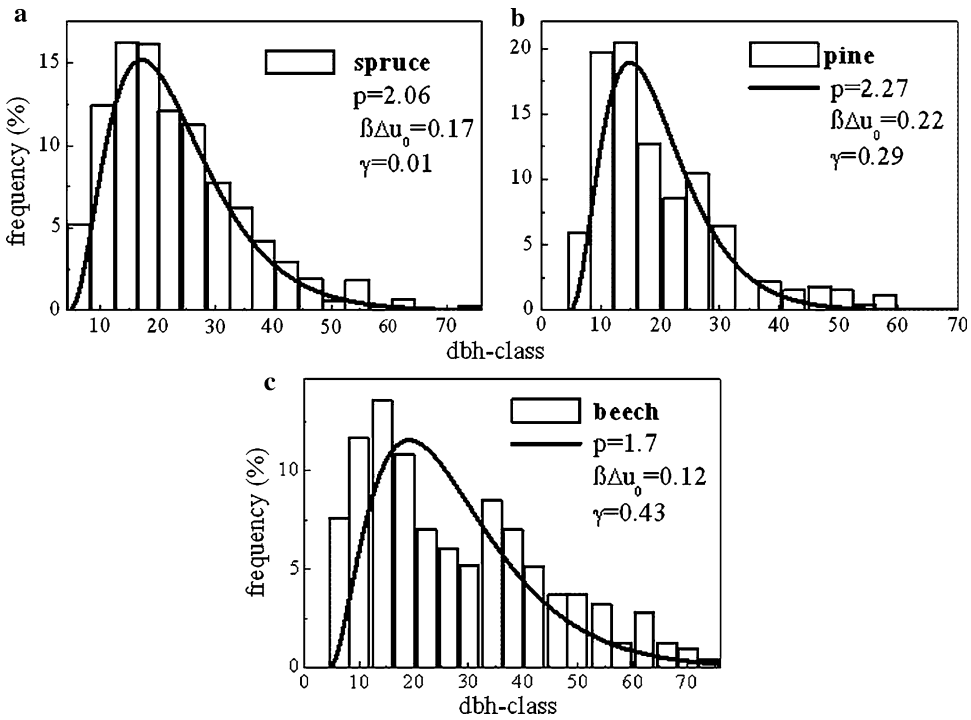

Fig. 11 *dbh*-frequency distributions of **a** spruce, **b** pine, **c** beech according to Fehrmann [38]. *Solid lines* are calculated with Eq. 1 and the parameters as indicated

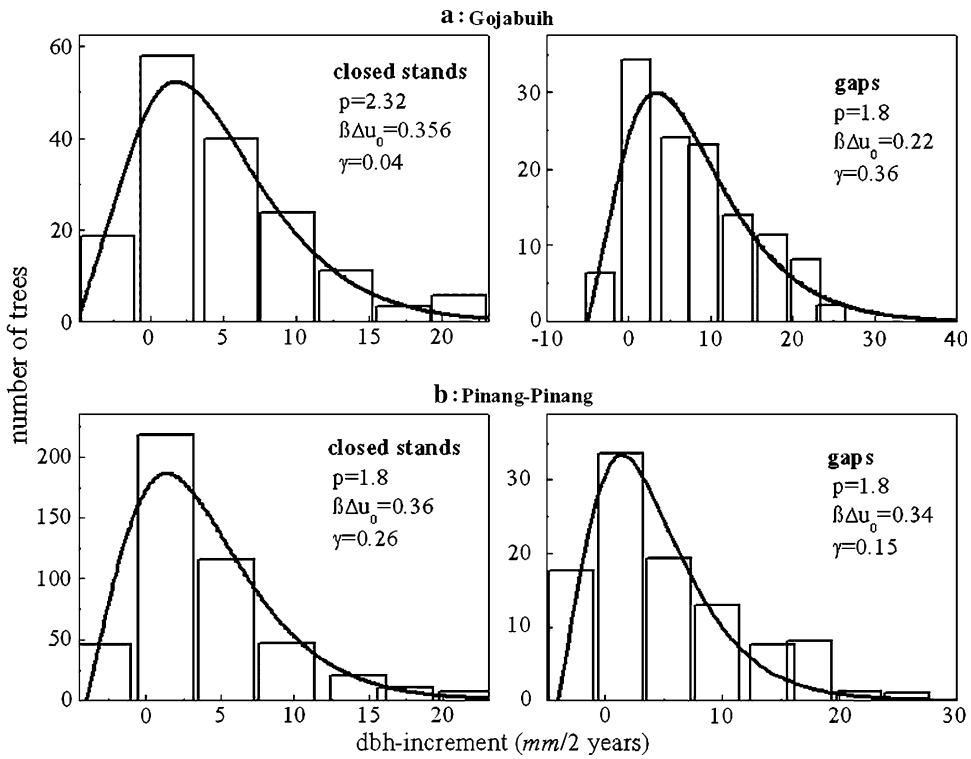

Fig. 12 Goyabuih and Pinang Pinang *dbh* frequency distribution according to Koyama and Hara [39]. Dates are presented in 2^n cm classes. Measurements were taken 2 years apart in closed stands and gaps in old-growth tropical foothill rain forests in West Sumatra. The *bold lines* are calculated with Eq. 1 and the parameters as inserted

An Important Example

We analyse mass distributions of *Xanthium strumarium* plants from a strand population studied by Weiner et al. [4]. In Fig. 7, the frequency distributions at five different ages are presented. The growth of meristem tissues via absorption of increments is fast in comparison with the structural organisation of the population. According to the IC model individual plants may thus be in an analogous situation as cells in a cell ensemble. Interactions among all individuals should thus optimize the superstructure of the population.

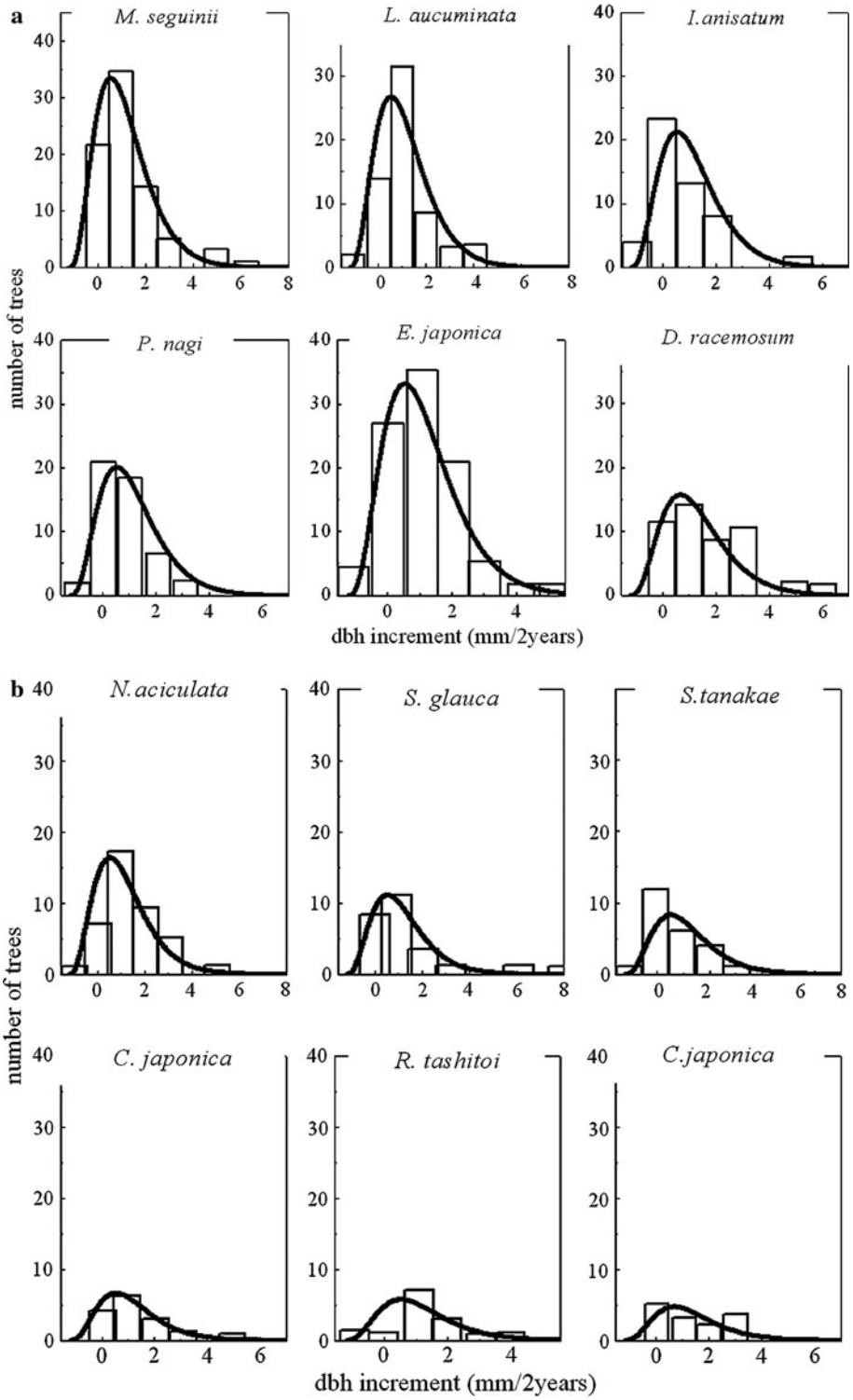

Fig. 13 **a**, **b** The frequency distributions of 2-year *dbh* increments (1981–1983) for cohorts of 12 abundant species growing in closed stands in a primary warm-temperature rain forest in the Segire basin, Yakushima Island according to Koyama and Hara [39]. The *bold lines* are calculated with Eq. 1 by using the parameters specified in the Tables 5, 6

This notion is checked by describing mass distributions of *X. strumarium* plants determined at different ages [4]. Non-linear fits using Eq. 1 lead to the solid lines in Fig. 7. Hence, these distributions are optimized patterns, where single plants, pairs and quadruples behave analogously (details not shown here). According to Fig. 8a the parameter p decreases during growth from $p = 3.05$ to $p = 0.4$. This evidences that during growth intracellular fluctuations freeze steadily. The line in Fig. 8a is calculated with the relation $3\left(1 - \sum h_y\left(\ln\left(\tau_{0y}\right), p = 3\right)X'_y\left(\omega_c\tau_y\right)\right)$ which is deduced from Eq. 8. The agreement shows that solidification of growing plants due to relaxation-frequency dispersion is related to the reduction of the intracellular dynamics.

Table 5 Growth-invariant parameters of the *dbh* increments as depicted in Fig. 13a

System	$\Delta\xi$ (2 years)
Myrsine seguinii	90
Litsea aucuminata	76.5
Illicium anisatum	60
Podocarpus nagi	54
Eurya japonica	90 ($\gamma = 0.1$)
Distylium racemosum	48

$p = 2.9$; $\beta\Delta u_0 = 1.67$; $\gamma = 0.11$

Table 6 Growth-invariant parameters of the *dbh* increments as depicted in Fig. 13b

System	$\Delta\xi$ (2 years)
Neolitsea aciculata	45
Symplocos glauca	31.5
Symplocos tanakae	31.5
Cleyera japonica	18
Rhododendron tashiroi	18
Camellia japonica	13.5

$p = 2.9$; $\beta\Delta u_1 = 1.67$; $\gamma = 0.11$

Table 7 $<p>$, $<\beta\Delta u_0>$ and $\Delta n'_{cc1}$ of the systems studied here

System	$<p>$	$<\beta\Delta u_0>$	$<\gamma>$
Diameter			
Coleus, cortex	1.88	0.10	0.21
Coleus, outskirt	1.85	0.042	0.25
Chenopodium	2.02	0.024	0.33
Spruce	2.06	0.17	0.01
Pine	2.27	0.22	0.29
Beech	1.7	0.12	0.43
Gojabuih	2.06	0.29	0.2
Pinang Pinang	1.8	0.28	0.37
Eurya japonica	2.9	1.61	0.11
Average	<2.06>	<0.32>	<0.26>
Height			
Chenopodium	0.87	0.065	0.38

Figure 8b illustrates that the width of the normalized distributions $n(\eta, p)/n_{\max}$ increases while p grows, indicating that the mixing entropy within the population increases.

Chenopodium album

We discuss now the description of diameter- and height-distributions of *Chenopodium album* in the vegetative regime as published by Nagashima et al. [36]. Figure 9 shows the diameter distributions at different initial densities. The solid lines are calculated with Eq. 1. The parameter p comes out to scatter around the mean value of $<p> \approx 2.02$. Apparently, the anisotropic structure in meristems reduces intracellular fluctuations [8]. At the highest density, the relative contact energy $\beta\Delta u_0$ drops to a low value [37].

Since an optimized superstructure is found in *C. album* diameter distributions, fluctuations and communication must be present in the population. Of course, aberrant data points come about when plants are clamped in unfavourable configurations. The linear deviations from the ideal state of reference are typified by $<\gamma> = 0.2$–0.4.

The height distributions in Fig. 10 are fitted with $p \approx 1$.

dbh Distributions

During secondary growth, woody stems show cambium-mediated radial expansion. Recently, the importance of transcriptional regulators, phytohormones and cell wall synthesis in secondary growth was demonstrated [37]. The formation of increments includes these processes.

*dbh*s are established growth parameters for trees: within a stem, the cylindrical cambium layer induces lateral broadening via cell multiplication accompanied by irreversible cell elongation into the longitudinal stem axis. A fraction of differentiated wooden cell layers develops while the bark is continuously reshuffled. The organisation within a stem runs fast compared to processes at the population level. Lateral growth can thus be described in terms of IC model. The *dbh* is consequently defined by $dbh \cong y$ whereby y is the number of ICs. Individual growing trees constitute a forest with an optimized superstructure.

dbh-Frequency Distributions in Beech, Spruce and Pine Forests

Satisfying reproductions of frequency distributions of stem *dbh* of spruce, beech and pine trees [38] are depicted in Fig. 11a–c. The solid lines are calculated with Eq. 1. The mean value of the parameter p is equal to $<p_{\exp}> = 2.01$ indicating reduced structural fluctuations in stem meristems, owing to the anisotropic configurations in which cells are assembled. Deviations due to aberrant data points are here again characterized by $\gamma = 0.24$. The increase of the contact energies: beach ($\beta\Delta u_0 = 0.09$; spruce, $\beta\Delta u_0 = 0.177$; pine, $\beta\Delta u_0 = 0.233$) goes along with decreasing shade tolerance.

Frequency Distributions of 2-Year *dbh*-Rates in the Old Natural Tropical Foothill Rain Forests, Gajbuih and Pinang Pinang

Natural rain forests comprised many species; they show closed stands and gaps [39]. Figure 12 shows the frequency distributions of *dbh* growth rates of Gajabuih and Pinang Pinang determined in 2^n mm classes by Koyama and Hara [39] in 1982 and 1984 in old tropical foothill rain forests.

The fit curves calculated with Eq. 1 and p values around two reproduce the observed distributions fairly well. The *dbh* growth rate and the absolute *dbh* classes are linearly correlated: during the relatively short span of growth, the initially optimized superstructure undergoes an affine transformation. The mean deviations induced by aberrant data points are $<\gamma> = 0.20$.

The Uniformity of the 2-Year *dbh* Growth Rates of 12 Abundant Species in a Tropical Rain Forest

The distributions of 2-year dbh increments (1981–1983) of cohorts of 12 different abundant species measured by Koyama and Hara [39] are shown in Fig. 13a, b. These 12 species represent 95% of the total number of trees. Since for low-abundance species data points are scarce, only the distribution of *Eurya japonica* was fitted by iteration. After scaling to the increment rate per 2 years [$\Delta\xi$ (2 yrs)],within the limits of accuracy the same pattern applies to all other species where $p = 2.9$ and $\beta\Delta u_0 = 1.67$ were left unchanged (Tables 5, 6).

Apparently, in warm-temperature rain forests [39] complex modes of interaction organise the 12 species into a superstructure whose members all show conformal distributions.

Final Comments

The IC model and the invariable presence of distribution patterns may be taken as an unmistakable manifestation of the elementary role of the entropy. Cell size-, biomass-, *dbh*- or growth-rate-distributions are all found to be optimized patterns. Moreover, according to Table 7, different species show nearly identical p values $<p> = 2.06$. The logistics of intracellular fluctuations should be the same.

During growth, the dynamics freezes, causing solidification as a consequence of relaxation-frequency dispersion. Maintaining stationary growth conditions requires perfect communication among the constituents at all levels, molecules, cells, tissue and organisms. Essentially the strikingly uniform growth-rate distributions of 12 abundant species in an undisturbed natural biotope point to highly cooperative modes of interaction that are not yet understood. Of course, deviations from the ideal line of growth are inevitable. Broad-band relaxation processes compensate for these "defects".

Objective evidence of a decisive influence of genetic factors is obtained from the description of bimodal growth curves: when vegetative growth is blocked, the coordinated activation of flowering-identity genes [27] is necessary to initiate the transition into the generative regime.

All in all, interpreting growth as an incremental process ruled by thermodynamics in both individuals and entire populations shows plant societies sharing their environment coordinately. In presence of unscheduled but perpetual constraints, resulting from genetic or exogenous causes, optimization at a modified state of reference allows even damaged plants to integrate into the whole ensemble. The community, in return, can readjust an ideal global configuration perhaps by exploiting unused resources. The good correspondence of observed patterns with the calculations indicates ecological integrity.

Appendix

Growth curves are calculated with Eq. 10. For biomass the parameter p was set equal to 3 while height was characterized by $p = 1$. All parameters except from p were assigned their values by educated guess and subsequent manual optimization.

To describe *dbh* or height distributions, Eq. 1 was subjected to an iterative non-linear fit procedure (Excel Solver). During iterations at constant values for ξ and $y_{\min}$ the parameters p and $\beta\Delta u_0$ were modified until the deviation reduction converged towards 0.0001. These fits incorporate aberrant data points. To quantify this, we use the parameter γ which relates all deviations from the ideal size-distribution to the total plant mass.

References

1. Bertallanaffy, V. L. (1957). Quantitative laws in metabolism and growth. *Quarterly Review of Biology, 32*, 217–231.
2. Schneider, M. K., Law, R., & Illian, J. B. (2006). Quantification of neighborhood-dependent plant growth by Bayesian hierarchical modelling. *Journal of Ecology, 94*, 310–321.
3. Hara, T. (1988). Dynamics of size structure in plant populations. *Trends in Ecology & Evolution, 3*, 129–133.
4. Weiner, J., Kinsman, S., & Williams, S. (1998). Modelling the growth of individuals in plant populations: local density variation in a strand population of *Xanthium strumarium* (*Asteraceae*). *American Journal of Botany, 85*, 1638–1645.
5. Weiner, J., & Thomas, S. W. (1986). Size variability and competition in plant monocultures. *Oikos., 47*, 211–222.
6. Banavar, J. R., Damuth, J., Maritan, A., & Rinaldo, A. (2002). Ontogenetic growth: Modelling universality and scaling. *Nature., 420*, 626–627.

7. Damgaard, C., Weiner, J., & Nagahshima, H. (2002). Modelling individual growth and competition in plant populations: growth curves of *Chenopodium album*. *Journal of Ecology, 90*, 666–671.
8. Jürgens, G. (2003). Growing up green: Cellular basis of plant development. *Mechanisms of Development, 120*, 1395–1406.
9. Green, P. B. (1976). Growth and cell pattern formation on an axis: Critique of concepts, terminology and modes of study. *Botanical Gazette, 137*, 187–202.
10. Cockcroft, C. E., den Boer, B. G. W., Healy, J. M. S., & Murrey, J. A. H. (2000). Cyclin D control of growth rate in plants. *Nature., 405*, 575–579.
11. Hara, T., & Yokozawa, M. (1994). Effects of physiological and environmental variations on size–structure dynamics in plant populations. *Annals of Botany, 73*, 39–51.
12. Schmid, I., & Kadzda, M. (2001). Vertical distribution and radial growth of coarse roots in pure and mixed stands of *Fagus sylvatica* and *Picea abies*. *Canadian Journal of Forest Research, 3*, 539–548.
13. Damgaard, C., & Weiner, J. (2008). Modeling of the growth of individuals in crowded plant populations. *J Plant Ecolology, 1*, 111–116.
14. Zeide, B. (1993). Analysis of growth equations. *Forest Science, 39*, 594–616.
15. Yeytman, B. A., & Cosgrove, D. J. (1998). A model of cell wall expansion based on thermodynamics of polymer networks. *Biophysical Journal, 75*, 2240–2250.
16. Kilian, H. G., Kemkemer, R., & Gruler, H. (2002). Universality and individuality as complementary factor to optimize and reproduce cell populations. *Colloid and Polymer Science, 280*, 1151–1156.
17. Kilian, H. G., Bartkowiak, D., Kaufmann, D., & Kemkemer, R. (2008). The general growth logistics of cell populations. *Cell Biochemistry and Biophysics, 51*, 51–66.
18. Kilian, H. G., Gruler, H., & Kemkemer, R. (2004). Relaxations processes during cell growth. *Progress in Colloid and Polymer Science, 125*, 198–205.
19. Pelling, A. E., Sehati, S. B., Gralla, B., Valentie, J. S., & Gimzewski, J. K. (2004). Local nanomechanical motion of the cell wall of *Saccharomyces cerevisae*. *Science., 305*, 1147–1150.
20. Volkov, I., Banavar, J. R., He, F., & Hubell, S. P. (2005). Density dependence explains tree species abundance and diversity in tropical forests. *Nature, 438*, 658–661.
21. Shemesh, T., Geiger, B., Bershatzky, A. D., & Kozlov, M. M. (2005). Focal adhesions as mechanosensors: A physical Mechanism. *Proceedings of the National Academy of Sciences of the United States of America, 102*, 12383–12388.
22. Sitte, P., Ziegler, H., Ehrendorfer, F., Bresinsky, A. (1997). *Strasburger, Lehrbuch der Botanik.* (34th ed., pp. 120, Fig. 1-42 B). Spektrum: Akademischer Verlag, Gustav Fischer.
23. Holmes, P., Goffard, N., Weiller, G. F., Rolfe, B. G., & Imin, N. (2008). Transcriptional profiling of *Medicago truncatula* root cells. *BMC Plant Biology, 8*, 21.
24. Micoulet, A., Spatz, J. P., & Ott, A. (2005). Mechanical response analysis and power generation by single-cell stretching. *Chemical Physics and Physical Chemistry, 6*, 663–670.
25. Koepf, M., & Kilian, H. G. (1999). Relaxation in the glass transition regime interpreted in terms of the aggregate model. *Acta Polymerica, 59*, 109–121.
26. Sitte, P., Ziegler, H., Ehrendorfer, F., & Bresinsky, A. (1997). *Strasburger, Lehrbuch der Botanik* (34th ed., pp. 400–411). Spektrum: Akademischer Verlag, Gustav Fischer.
27. Penel, C., Gaspae, Th, & Geppin, H. (1985). Rapid interorgan communications in higher plants with special reference to flowering. *Biologia Plantarium., 27*, 334–338.
28. Puig, S., Mira, H., Dorcey, E., Sancenón, V., Andrés-Colás, N., Garcia-Molina, A., et al. (2006). Higher plants possess two different types of ATX1-like copper chaperones. *Biochemical and Biophysical Research Communications, 354*, 385–390.
29. Mackenzie, S., & McIntosh, L. (1999). Higher plant mitochondria. *Plant Cell, 11*, 571–585.
30. McCrum, N. G., Read, B. E., & Williams, G. (1967). *Anelastic and dielectric effects in polymer solids* (p. 102). London: Wiley.
31. Brophy, C., Gibson, D. J., Wayne, P. M., & Connolly, J. (2008). How reproductive allocation and flowering probability of individuals in plant populations are affected by position in stand size hierarchy, plant size and CO_2 regime. *J Plant Ecology, 1*, 207–215.
32. Hofmann, A. L. (2007). *Untersuchungen zur Isolierung von Regulator-Genen des floralen Meristem-Identitäts-Gens FLORICAULA aus Antirrhinum majus* (Thesis). (pp. 13–15) Köln: Matematisch-Naturwissenschaftliche Fakultät, Universität.
33. Ogle, K., & Pacala, S. W. (2009). A modeling framework of inferring tree growth and allocation from physiological, morphological and allometric traits. *Tree Physiology, 29*, 587–605.
34. Hozumi, K. (1987). Analysis of growth curve of stem volume in some woody species using the *u–w* diagram. *The Botanical Magazine Tokyo, 100*, 87–97.
35. Nagashima, H., Tereashima, I., & Katoh, S. (1995). Effects of plant density distributions of plant height in chenopodium album stands: analysis based on continuous monitoring of height-growth of individual plants. *Annals of Botany, 75*, 173–180.
36. Nagashima, H., & Terashima, I. (1995). Relationships between height, diameter and weight distributions of *Chenopodium album* plants in stands: effects of dimension and allometry. *Annals of Botany, 75*, 181–188.
37. Groover, A., & Robischon, M. (2006). Developmental mechanisms regulating secondary growth in woody plants. *Current Opinion in Plant Biology, 9*, 55–58.
38. Fehrmann, L. (2006). Alternative Methoden zur Biomassenschätzung auf Einzelbaumebene unter spezieller Berücksichtigung der k-Nearest Neighbour (k-NN) (Thesis). (pp. 59) Göttingen: Methode Fakultät für Forstwissenschaften und Waldökologie der Georg-August-Universität.
39. Koyama, T., & Hara, T. (1989). Frequency distribution of tree growth rate in natural forest stands. *Annals of Botany, 64*, 47–57.